ISSN: 1983 7402 ITA, 27 a 29 SET 2022

Helicopter firing-rocket performance and pilot´s workload evaluation from flight data

Raphael Gomes Cortes[1], Luiz Fabiano Damy[1], and Emilia Villani[1]
[1]Aeronautics Institute of Technology , São José dos Campos/SP - Brazil

***Abstract*— Rocket air-to-ground shot is typically evaluated in a fixed ground facility, where the ground impact point is estimated. A methodology with no ground infrastructure was proposed to estimate the unguided rocket impact point and to assess the pilot's workload on the ramp and low-level maneuvers. Formulations implemented used Haversine, Bearing and Destination navigation formulas, two degrees of freedom rocket model, and the rotor downwash is modeled based on momentum and blade element theory. Results have shown an estimation of the impact point lower than six meters and coherent performance metrics when comparing ramp and low-level maneuvers.**

***Keywords*— Evaluation, Helicopter, Rocket.**

I. Nomenclature

A_r :	Rotor disc area
A_{rkt} :	Rocket section are. Thusa
C_d :	Drag Coefficient
d_{Impact} :	Distance from ground rocket impact to aircraft
dl :	Lateral distance rocket deviation due to wind
d_{Plan} :	Distance from rocket impact to aircraft (reference plane)
d_{Ref} :	Distance from target ground reference to aircraft
D :	Drag force of rocket
F_n :	Normal force in rocket at launcher
h_{Shot} :	Shot height
h_{Rkt} :	Rocket trajectory height
h_T :	Terrain height
m :	Rocket mass
$M_{aircraft}$:	Aircraft mass
M_a :	Mach number
r :	Distance from the rotor radius center
R :	Rotor radius
t :	Perpendicular axes at rocket reference
T :	Thrust force of rocket
T_a :	Ambient air temperature
T_s :	Standard temperature at a altitude
u :	Horizontal axial axes at rocket reference
V_0 :	Rocket true airspeed
V_c :	Calibrated airspeed
V_g :	Ground speed
v_{i0} :	Induced velocity in hover flight
v_i :	Non-uniform induced velocity in forward flight
v_{ih} :	Induced velocity in forward flight
v_{id} :	Induced velocity in descend flight
V_z :	Vertical speed of the aircraft
v :	Vertical axes at rocket reference
$Wind$:	Local wind
Z_{pShot} :	Shot flight altitude
$Z_{pTarget\,Ref}$:	Target reference plan altitude
β :	Bearing angle (relative to true North)
ψ :	Heading angle (relative to magnetic North)
Δt :	Time increment
Δw :	Lateral angle rocket deviation due to wind
ΔZ_{pError}	Altimeter correction factor
θ :	Pitch angle of rocket
$\theta_{Aircraft}$:	Pitch angle of aircraft
$\theta_{Launcher}$:	Pitch angle of launcher relative to airframe
Ψ :	Azimuth angle of rotor blade
ρ :	Air density

Cortes, R., cortes@ita.br; ; Damy, L., damy@ita.br; Villani, E., evillani@ita.br.

II. Introduction

High Armed Forces Staff Command needs to keep the pilots' operational level at a high level of training because flight maneuvers rely on individual performance. Thus, continuous training is performed to acquire the required cognitive skill levels. Indeed, is necessary to measure the accuracy of weapons systems and evaluate the performance of the pilots, which is done by using a standard rocket fire test facility in a triangular configuration, where one vertex is the target, and the others have optical observation towers. These tower measurements, together with the knowledge of the distances to the target, provide the coordinates of the actual impact point [1]. Nevertheless, is not always possible to use this kind of facility; thus is proposed to measure the accuracy of shots using available rocket and flight data in addition to video recorded from an eye tracker device.

Regarding pilot workload, there is no standard methodology applied for helicopter shots, thus was proposed to use as reference rifleman stability shot parameters to assess pilot performance on the shot maneuver ([2], and [3]). In this, the shot stability is measured as the target's area of the aiming points. Another parameter analyzed was the deviation of the maneuver parameters [4], which was called F-score.

The methodology proposed, using well-known formulations, was applied in the ramp and low-level air-to-ground shot maneuvers. Based on the flight data and momentum and blade element theory, initial rocket conditions were calculated. Then, using a rocket trajectory model with two degrees of freedom, the impact point coordinates, and the workload parameters were estimated with navigation formulas (Haversine, Bearing and Destination). Putting these coordinates into a digital map, the terrain impact point could be determined and validated with video data from eye-tracker glasses.

III. Materials and methods

A. Scenario

The measurements of unguided rocket fire shots occurred during an air-to-ground rocket-firing campaign from the Brazilian Army Aviation. Usual weapons delivery profiles are Diving Fire (ramp), Running Fire, Hover Fire, and Low Altitude Pop-up Fire (low-level), as given in [5]. The profiles analyzed were the ramp and low-level that are presented in Figure 1. The ramp maneuver starts from a level flight. Then the aircraft dives towards the target, where the pilot aims. In the low-level maneuver, the pilot navigates close to the ground and near the target, rapidly ascends, reverts the aircrafts attitude, and starts aiming to perform the shot. These maneuvers were performed in daylight visual conditions and at night-time using night vision goggles (NVG).

During the aiming phase, the pilot must search for previously established values of airspeed (V_c), height above ground (h_{Shot}), and distance (d_{Plan}), which are maneuvers parameters, and adjust the horizontal attitude towards the target, compensating for positioning errors, seconds before the shot event.

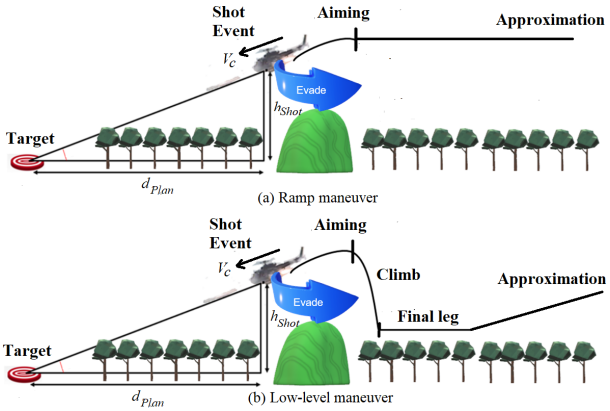

Fig. 1. Rocket shot maneuvers.

Two rounds of ramp maneuver shots and two rounds of low-level maneuver shots were used for analysis and, in all cases, in daylight conditions. Rocket firing was carried out only on the left side of the aircraft.

B. Apparatus

The aircraft used in rocket firing training was the AS550A2 Fennec AvEx model in the armed configuration, as illustrated in Figure 2, with a projected aiming sighting system.

Fig. 2. AS550A2 Fennec AvEx in armed configuration.

This aircraft was dual pilot operated with stability augmented systems to compensate for helicopter instability in pitch and roll movements. Flight Data was recorded from the aircraft system for post-flight analysis at a sampling rate of 4 Hz.

In this study, the entire flight was recorded for analysis using Tobii Pro Glasses 2, presented in Figure 3, which has a front camera that records the image in front of the individual, two cameras facing each eye, a gyrometer, an accelerometer, and a microphone to capture ambient audio.

Fig. 3. Eye tracker model Tobii Pro Glasses 2.

An eye tracker camera was used to get the coordinates of the rocket impact point to validate the proposed methodology. The latitude and longitude of the rocket point of impact were estimated using video ground references and obtained using the free software Google Earth Pro.

C. Data Analysis

The general schematic of the data analysis flown is presented in Figure 4, where the principal flight data used were: flight altitude (Z_p), ambient air temperature (T_a), calibrated airspeed (V_c), Heading angle (ψ), pitch angle (θ), aircraft mass ($M_{aircraft}$), Latitude (Lat) and Longitude (Lon).

The Navigation calculation used Haversine Formula, Bearing, and Destination functions, which consider the Earth a great circle, which are more straightforward for implementation and have a slight error for short distances. These formulas were necessary for computing ground speed, lengths, and estimated coordinates.

Helicopter rotor downwash flight has an initial interference in the rocket trajectory; this inflow was computed using blade element theory, including theoretical and empirical adjustments to capture complexities, non-uniform inflow, and skew angle wake. As the shots are performed in stable conditions, the hypothesis assumed that this theory could predict the mean value of this downwash.

Rocket motion analysis was performed using two degrees of freedom model with heading correction using rocket manufacturer tables due to wind. The two degrees of freedom model simplifies the six degrees of freedom model but retains the range and height estimation and is more suitable for the available data.

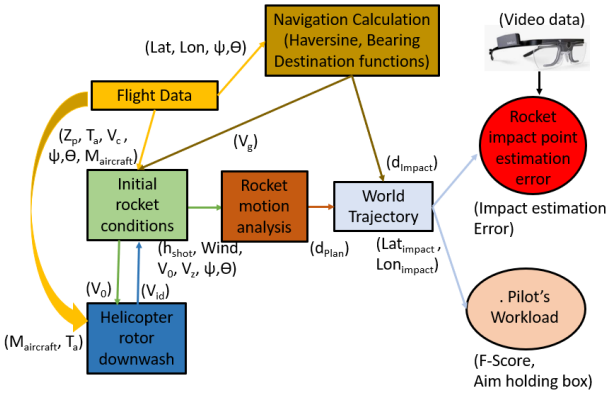

Fig. 4. General schematic of data analysis.

1) Navigation Calculations: Using the latitude (Lat) and longitude (Lon) coordinates data and the great circle method, it is possible to obtain the distance between two coordinates, the bearing angle relative to the true north and the destination point given an origin coordinate, a bearing and distance to travel, as illustrated in Figure 5.

The Haversine formula ([6], and [7]) was used calculate distances between two coordinates on Earth, as given in (1), and (2), which q is an auxiliary variable. The $arctan2(y, x)$ function computes the arc tangent of the ratio y/x in all four trigonometric quadrants from $-\pi$ to π.

$$Hav(\begin{bmatrix} Lat_1 \\ Lon_1 \end{bmatrix}, \begin{bmatrix} Lat_2 \\ Lon_2 \end{bmatrix}) = 12742 \cdot arctan2(\sqrt{q}, \sqrt{1-q}) \quad (1)$$

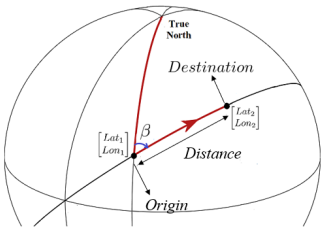

Fig. 5. Navigation Calculations.

$$q = sin^2(\frac{\Delta Lat}{2}) + cos(Lat_1) \cdot cos(Lat_2) \cdot sin^2(\frac{\Delta Lon}{2}) \quad (2)$$

The bearing angle (β) between two coordinates ([7], [8], and [9]) can be calculated as given in (3).

$$\beta = atan2(sin(\Delta Lon) \cdot cos(Lat_2), \\ cos(Lat_1) \cdot sin(Lat_2) - sin(Lat_1) \cdot cos(Lat_2) \cdot cos(\Delta Lon)) \quad (3)$$

Destination function ($Destination$) ([7], and [8]) calculates a final position given a distance and bearing from a starting point defined by latitude and longitude, along a great circle model, given by (4) and (5).

$$Lat_2 = asin(sin(Lat_1) \cdot cos(\frac{distance}{6137 \cdot 10^3}) + \\ cos(Lat_1) \cdot sin(\frac{distance}{6137 \cdot 10^3}) \cdot cos(\beta)) \quad (4)$$

$$Lon_2 = Lon_1 + atan2(sin(\beta) \cdot sin(\frac{distance}{6137 \cdot 10^3}) \cdot cos(Lat_1), \\ cos(\frac{distance}{6137 \cdot 10^3}) - sin(Lat_1) \cdot sin(Lat_2)) \quad (5)$$

2) Initial rocket conditions: The shot height (h_{Shot}) is computed through formula given by (6), where flight altitude (Z_{pShot}) is subtracted by altitude of target reference plan ($Z_{pTarget\,Ref}$) and added by an altimeter correction factor (ΔZ_{pError}). This altimeter correction factor was calculated only once to compensate for anemometric system errors to achieve the radar-altimeter height verified on the eye tracker video.

$$h_{Shot} = Z_{pShot} - Z_{pTarget\,Ref} + \Delta Z_{pError} \quad (6)$$

Initial rocket attitude is given by aircraft attitude ($\theta_{Aircraft}$) added by launcher attitude relative angle to the airframe ($\theta_{Launcher}$).

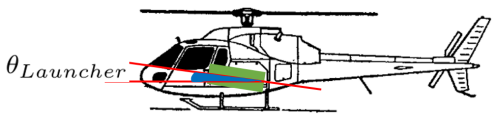

Fig. 6. Launcher attitude relative angle to the airframe.

The initial shot bearing angle (β_{shot}), as shown in Figure 7, relative to true North is computed as indicated in (7), as a function of the aircraft magnetic heading (ψ_{shot}) and the magnetic deviation. The magnetic variation is determined depending on the flight location.

$$\beta_{Shot} = \psi_{Shot} + Magnetic\,Deviation \quad (7)$$

The vertical shot speed was calculated using the variation of altitude over time (ΔZ_p), as indicated in [10], corrected by ambient temperature (T_a) and standard temperature at an altitude (T_s), as given by (8).

$$V_z = \left(\frac{T_a + 273.15}{T_s + 273.15}\right) \frac{\Delta Z_p}{\Delta t} \quad (8)$$

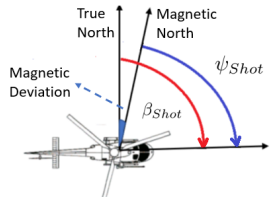

Fig. 7. Heading and bearing angle relations.

Aircraft true airspeed (V_0) was calculated as given by (9), as indicated in [10], as a function of calibrated speed (V_c) and density ratio (σ). The density ratio (σ) is determined by [10].

$$V_0 = \frac{V_c}{\sqrt{\sigma}} \quad (9)$$

$$\sigma = \left(\frac{T_a + 273.15}{288.15}\right) \cdot \left(1 - \left(\frac{0.00198}{288.15} Z_{p\,Shot}\right)\right)^{-5.2593} \quad (10)$$

Aircraft ground speed (V_g) was calculated from the distance between two latitude (Lat) and longitude (Lon) coordinates given by Haversine (Hav) formulas (1) and (2) divided by the corresponding time interval, and the bearing angle (β_g) using (3).

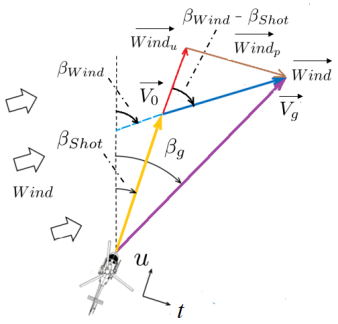

Fig. 8. Wind calculation.

Wind at the shot moment is computed by the vector difference between the ground speed (V_g) and true speed (V_0) referenced to the true north, as can be seen in Figure 8. Thus wind can be decomposed into one component in the horizontal displacement of the rocket ($Wind_u$), given by (11), and another perpendicular to this displacement ($Wind_t$), computed from (12).

$$Wind_u = Wind \cdot cos(\beta_{Wind} - \beta_{Shot}) \quad (11)$$

$$Wind_t = Wind \cdot sin(\beta_{Wind} - \beta_{Shot}) \quad (12)$$

3) Helicopter rotor downwash: It is necessary to compute rotor downwash, which is the wind flow velocity induced by the rotor blades rotation; this wake is also known as inflow. From the momentum theory [11], the rotor downwash in the particular hover case is given by (13). In this equation, $M_{Aircraft}$ is the aircraft mass, g is the gravitational acceleration, ρ is the air density, and A_r is the rotor area.

$$v_{i0} = \sqrt{\frac{M_{Aircraft} \cdot g}{2 \cdot \rho \cdot A_r}} \quad (13)$$

For forward flight, the inflow becomes non-uniform due to the interactions of airspeed and rotating blades. Thus, a simple model that takes this non-uniformity into account is

proposed by [11], where an increasing inflow across rotor diameter is generated as given in (14). As the launcher is at the advancing blade side, a blade azimuth equal to $\Psi = 150^o$ and the corresponding distance r from the rotor center were chosen for computing the mean downwash.

$$v_i = v_{i0}\left[1 + 1.21\left(\frac{r}{R}\right)cos(\Psi)\right] \tag{14}$$

A formulation proposed by [11], that assumes a cylindrical wake, was used to take into account the fact that the inflow is oblique to the rotor disc and is given by (15).

$$v_{ih} = V_0\left(\left(\frac{1}{2} + \left(\frac{v_i}{V_0}\right)^2\right)^2 - \frac{1}{4}\right)^{-\frac{1}{4}} \tag{15}$$

An illustration of non-uniform downwash heatmap and oblique downwash in forward flight is presented in Figure 9.

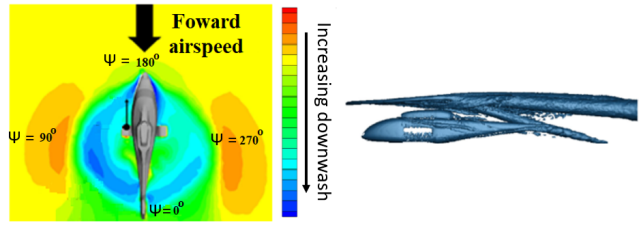

Fig. 9. Illustration of non-uniform and oblique downwash [12].

As the helicopter in the shot moment is not necessary at a level flight, the vertical downwash component v_{id}, as indicated in [11], is estimated solving equation (16), using the aircraft rate of descending V_Z and the estimated inflow v_{ih} in the level flight.

$$\left(\frac{v_{id}}{v_{ih}}\right)^4 - 2\left(\frac{V_z}{v_{ih}}\right)\left(\frac{v_{id}}{v_{ih}}\right)^3 + \left(\frac{V_z^2}{v_{ih}^2} + \frac{V_0^2}{v_{ih}^2}\right)\left(\frac{v_{id}}{v_{ih}}\right)^2 - 1 = 0 \tag{16}$$

4) Rocket motion analysis: To calculate rocket trajectory, a set of two degrees of freedom equations from the rocket´s parallel-perpendicular frame [13] was decomposed in the $u-v$ plane as indicated in Figure 10.

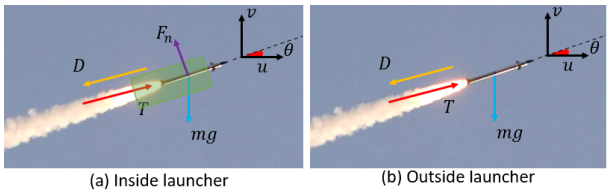

Fig. 10. Forces applied in the rocket.

While the rocket is inside the launcher (Figure 10(a)) a normal force (F_n) given by (17) was applied. When the rocket leaves the launcher, this force becomes zero. In this formulation, the rocket mass (m) was linearly reduced during the thrust phase.

$$F_n = m \cdot g \cdot cos\theta \tag{17}$$

For rocket drag profile, data from similar rocket-like bodies was used as presented in [14], where the drag coefficient (C_D) is a function of Mach number (M_a), which is the ratio of airspeed and the speed of sound. Still, the effect of the angle of the attack or side slip angle was not considered. According to [14], the C_D for the power-off period was obtained from the flight test, and the C_D for the power-on period was determined by adjusting the base pressure drag. Then, drag force ($D(t)$) was calculated as (18). It used available manufacture rocket data for the thrust curve over time ($T(t)$).

$$D(t) = \frac{1}{2} \cdot C_d(M_a) \cdot \rho \cdot A_{rkt} \cdot (\dot{u}^2(t) + \dot{v}^2(t)) \tag{18}$$

The resultant forces about u and v axis are denoted by (19) and (20) respectively, where all variables are function of time. The initial conditions are given by (21), with horizontal velocity $\dot{u}(0)$ as the aircraft's true airspeed (V_0) and vertical speed $\dot{v}(0)$ computed as the relative difference between downwash (v_{id}) and rate of descend. (V_z)

$$\frac{\mathrm{d}^2u}{\mathrm{d}t^2} = \frac{T}{m} \cdot cos(\theta) - \frac{D}{m} \cdot cos(\theta) - \frac{F_n}{m} \cdot sin(\theta) \tag{19}$$

$$\frac{\mathrm{d}^2v}{\mathrm{d}t^2} = \frac{T}{m} \cdot sin(\theta) - \frac{D}{m} \cdot sin(\theta) - g + \frac{F_n}{m} \cdot cos(\theta) \tag{20}$$

$$\begin{cases} u(0) = 0,\ v(0) = h_{shot} \\ \dot{u}(0) = V_0,\ \dot{v}(0) = v_{id} - V_z \\ \theta(0) = \theta_{aircraft} + \theta_{launcher} \end{cases} \tag{21}$$

Model rocket trajectory updates were computed over time increment until ground level was reached, given by equations to (22) to (24).

$$\begin{bmatrix}\dot{u}(t+1)\\ \dot{v}(t+1)\end{bmatrix} = \begin{bmatrix}\dot{u}(t)\\ \dot{v}(t)\end{bmatrix} + \begin{bmatrix}\ddot{u}(t)\\ \ddot{v}(t)\end{bmatrix}\Delta t \tag{22}$$

$$\begin{bmatrix}u(t+1)\\ v(t+1)\end{bmatrix} = \begin{bmatrix}u(t)\\ v(t)\end{bmatrix} + \begin{bmatrix}\dot{u}(t) + Wind_u\\ \dot{v}(t)\end{bmatrix}\Delta t \tag{23}$$

$$\theta(t+1) = arctan(\frac{\dot{v}(t)}{\dot{u}(t)}) \tag{24}$$

5) World Trajectory: With rocket trajectory determined, it is placed on the digital map, using data of shot latitude (Lat_{Shot}), shot longitude (Lon_{Shot}), shot bearing (β_{Shot}), and shot trajectory curve.

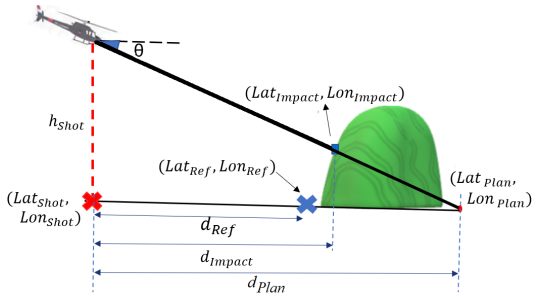

Fig. 11. Impact calculation.

Distances must be converted into Latitude and Longitude, using Haversine formula (presented in (1), and (2)) and destination function (presented in (4), and (5)). Therefore the impact point at the reference terrain plan (Lat_{Plan}, Lon_{Plan}) is calculated as given by (25).

$$\begin{bmatrix}Lat_{Plan}\\ Lon_{Plan}\end{bmatrix} = Destination(\begin{bmatrix}Lat_{Shot}\\ Lon_{Shot}\end{bmatrix}, \beta_{Shot}, d_{Plan}) \tag{25}$$

To estimate the impact location, as shown in Figure 11, is necessary the find out the minimum difference between rocket

trajectory height (h_{Rkt}) and terrain height (h_T), as given by formulas (26) to (29).

$$\begin{bmatrix} Lat_i \\ Lon_i \end{bmatrix} = Destination(\begin{bmatrix} Lat_{Shot} \\ Lon_{Shot} \end{bmatrix}, \beta_{Shot}, d_i) \quad (26)$$

$$d_i \epsilon [d_{Ref}; d_{Plan}] \quad (27)$$

$$d_{Impact} = argmin_{d_i}(h_{Rkt}(Range_{Rkt} - d_i) - h_T(\begin{bmatrix} Lat_i \\ Lon_i \end{bmatrix}) \quad (28)$$

$$\begin{bmatrix} Lat_{Impact} \\ Lon_{Impact} \end{bmatrix} = Destination(\begin{bmatrix} Lat_{Shot} \\ Lon_{Shot} \end{bmatrix}, \beta_{Shot}, d_{Impact}) \quad (29)$$

To take into account perpendicular wind effect on the trajectory, as indicated in Figure 12, the correction for the lateral deviation correction (dl) of the rocket's specification was included using look-up interpolation table (C) as a function of shot height (h_{solo}) and initial rocket attitude ($\theta_{Aircraft} + \theta_{Launcher}$), the result is given by (30). After determining lateral deviation, the formulations from (26) to (29) should be repeated, changing β_{Shot} by $\beta_{Shot} + \Delta w$ to find the estimated rocket impact on ground.

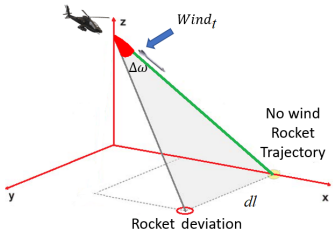

Fig. 12. Rocket deviation due to wind .

$$\Delta w = \frac{dl}{d_{Impact}} = \frac{C(h_{solo}, \theta_{Aircraft} + \theta_{Launcher}) Wind_t}{d_{Impact}} \quad (30)$$

6) Pilot´s workload: To assess pilot workload in the shot maneuver was used as reference rifleman stability shot parameters ([2], and [3]). In this, is measured the aiming points area estimated on the target two seconds prior shot event.

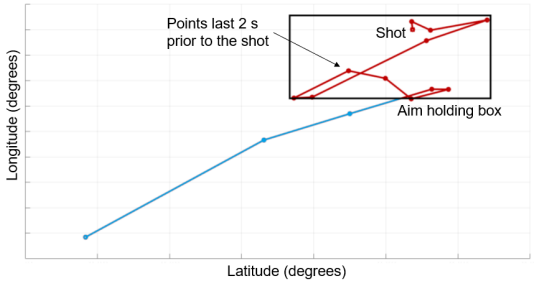

Fig. 13. Aiming holding box prior to shot.

Another flight workload score calculated was the deviation of the maneuver aiming parameters (F) at the shot moment, given by (31), defined as F-score [4]. This parameter is determined using airspeed $\overline{\Delta V_c}$, height above ground $\overline{\Delta h_{Shot}}$, and distance $\overline{\Delta d_{Impact}}$, where $\overline{\Delta X}$ is then normalized by the maximum X deviation expected given by (32). The higher the score, the better the pilot´s performance in acquiring maneuver parameters.

$$F = 3 - (\overline{\Delta V_c} + \overline{\Delta h_{Shot}} + \overline{\Delta d_{Impact}}) \quad (31)$$

$$\overline{\Delta X} = \frac{X_{Deviation\ from\ maneuvre\ reference}}{X_{Maximum\ acceptable\ deviation}} \quad (32)$$

IV. Results and Discussion

A. Rocket impact point estimation error

The final result of the proposed methodology with a rocket model with two degrees of freedom is shown in Figure 14, where the estimated impact point and the visual impact point are indicated.

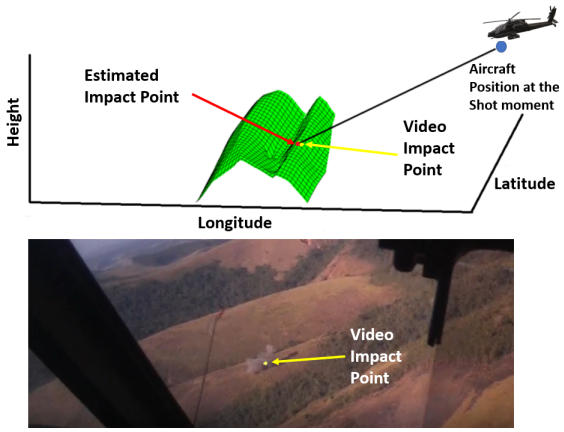

Fig. 14. Rocket impact estimation.

The estimated rocket impact points are presented in Table I, where an absolute error lower than six meters was achieved in random directions.

TABELA I

Impact point estimation error

Point	Maneuver	Error (m)
1	Ramp	5.3
2	Ramp	5.6
3	Low-Level	5.8
4	Low-Level	4.6

The visual measure warhead detonation area had a radius of ten meters around the visual impact point. Thus, an error of six meters has a low impact on the estimated damage intent on the target. This error could be reduced using a higher fidelity rocket and downwash data. Besides that, there is a gain for the operator as rockets tables usually do not provide a calculus for random attitude, height, and rate of descent.

In the built model, it was found that the helicopter rotor downwash reduces the rocket range with front wind, as present in [12], and this estimate is crucial to reduce the overall error of the rocket impact position. As the data is from the left launcher (advancing blade), it must be evaluated if the model obtains the same error level at the right launcher.

This methodology achieved good results in predicting the impact point of the first rocket shot; in the case of a burst of rockets, the wake of the first rocket causes a trajectory modification that is not implemented in this model.

With more rocket and aircraft data available, a comprehensive analysis could be made; for instance in [12], a six degrees of freedom rocket model was built with a computational fluid dynamics (CFD) downwash rotor model. More complex models require more specific data that sometimes are not completely available, so one approach could be to calibrate

an armed forces model after each shot campaign until a lower level of precision is reached.

This type of methodology, when validated at daylight maneuver, could be used to predict night shots using NVG since the impact point could not be easily identified. No ground infrastructure was needed to estimate the impact points, and the target must not be a flat surface.

A more significant number of shots could be used to calculate the probable circular error and other metrics that help estimate the firepower of the attack mission to the Armed Forces General Staff Command.

B. Pilot´s workload

The pilot workload metrics are presented in Table II, with the aim holding box normalized by the shots mean area.

TABELA II

PILOT MANEUVER PERFORMANCE METRICS

Point	Maneuver	F-Score	Aim holding box area normalized
1	Ramp	2.3	1.3
2	Ramp	1.7	1.2
3	Low-Level	0.94	0.9
4	Low-Level	0.31	0.5

As expected, the ramp maneuver got a higher F-score than the low-level maneuver; as in the ramp maneuver, the shot is done in more stabilized conditions, and the pilot has more time to acquire the maneuver parameters. Even though the pilot did not follow the exact maneuver parameter in the low-level operational maneuver, the target was hit at similar positions.

Regarding the aim holding box, the value in the ramp maneuver is also higher than in the low-level maneuver. This also indicates that the shot was done at stable conditions. Thus, the pilot waited for a better moment to shoot (larger aim holding box). On the other hand, in the low-level case, the pilot has less time to aim at the target, and more handling is needed (low value for the aim holding box). Indeed, fewer checks of the maneuvers parameter are made (low F-score).

The ramp maneuver is known qualitatively as a primary shot training maneuver because it demands less pilot workload than the low-level maneuver, as reflected by the data analyzed.

These pilot workload metrics could be analyzed together with physiological sensors, which could be important for improving flight safety, reviewing doctrine, and validating the feasibility of flight simulator training [15]. High levels of cognitive demand can lead to errors with catastrophic outcomes. Thus this knowledge can help avoid errors. This could establish the minimum acceptable training parameter for the shot precision and the pilot performance during the aiming phase.

V. CONCLUSION

The purpose of this work was to evaluate pilot performance on the helicopter shot of an unguided rocket. A two-degree-of-freedom rocket model methodology was applied to helicopter flight data, using an eye tracker video recorded as a validation method. The methodology used does not require any ground infrastructure, compared with a standard rocket shot facility, and was able to evaluate the estimated impact point and pilot workload independently of the local, light (day or night), and terrain conditions.

Rocket impact points could be estimated with less than six meters of error, in random directions, in an irregular terrain. Regarding the workload metrics, the results show that the ramp maneuver demands less pilot workload than the low-level maneuver and is coherent with known qualitative evaluations. These data obtained can provide metrics to Armed Forces General Staff Command on the weapon system's efficiency and the pilot training level.

Future works in this area should evaluate more fidelity or complex rocket models and downwash models to reduce the error in the impact point prediction in both left and right launchers, as the rotor inflow is not symmetric. Regarding the pilots performance, the relationship of the aircraft handling in the aiming phase with physiological sensors and their possible applications in pilot training should be studied. In this work, the wind was computed using a deterministic approach using the available flight data. Otherwise, uncertainties in the aiming point could be quantified using probabilistic models for parameters. As an example, the wind could be modeled as a random variable.

VI. ETHICS STATEMENTS

The experimental protocol was reviewed by the ethics committee with the global objective of the investigation of physiological data variables on pilot activity.

REFERENCES

[1] L. F. Damy, "Uma metodologia de emprego de armamento ar-solo para a Aviação do Exército," 2009.

[2] S. A. Brown and K. B. Mitchell, "Shooting stability: A critical component of marksmanship performance as measured through aim path and trigger control," vol. 2017-October. Human Factors an Ergonomics Society Inc., 2017, pp. 1476–1480.

[3] P. D. Espinosa, S. O. Nagashima, G. K. W. K. Chung, and E. L. Baker, "Development of sensor-based measures of rifle marksmanship skill and performance. cresst report 756," 2009.

[4] H. Jin, Z. Hu, K. Li, M. Chu, G. Zou, G. Yu, and J. Zhang, "Study on how expert and novice pilots can distribute their visual attention to improve flight performance," *IEEE Access*, vol. 9, pp. 44 757–44 769, 2021.

[5] T. B. Meriç, "An active rocket launcher design for an attack helicopter a thesis submitted to the graduate school of natural and applied sciences of middle east technical university," pp. 1–71, 2018.

[6] P. Soares, "Flight data monitoring and its application on algorithms for precursor detection aerospace engineering examination committee," 2014.

[7] C. Veness, "Calculate distance and bearing between two latitude/longitude points using haversine formula in javascript," 2022. [Online]. Available: https://www.movable-type.co.uk/scripts/latlong.html

[8] E. Williams, "Aviation formulary v1.47," 2013. [Online]. Available: https://edwilliams.org/avform147.htm

[9] R. Bullock, "Great circle distances and bearings between two locations," 2007.

[10] USNTPS, "United States Naval Test Pilot School- flight test manual - 106," pp. 1–562, 1996.

[11] A. K. Cooke and E. W. H. Fitzpatrick, "Helicopter test and evaluation," 1994.

[12] H. Kim and K. Yee, "Downwash effect on the unguided rocket under rotor wake and external wind," *Transactions of the Japan Society for Aeronautical and Space Sciences*, vol. 63, pp. 80–89, 2020.

[13] Z. Doucet, "Multistage 2-dof rocket trajectory simulation program for multistage 2-dof rocket trajectory simulation program for freshmen level engineering students freshmen level engineering students," 2019. [Online]. Available: https://scholarsjunction.msstate.edu/td/3252

[14] W. Charubhun, P. Chusilp, and N. Nutkumhang, "Effects of aerodynamic coefficient uncertainties on trajectory simulation of a short-range solid propellant free rocket," *26th Internetional Symposium on Ballistics*, 9 2011.

[15] S. Magnusson, "Similarities and differences in psychophysiological reactions between simulated and real air-to-ground missions," *International Journal of Aviation Psychology*, vol. 12, pp. 49–61, 2002.